A Letters Journal Exploring the Frontiers of Physics

October 2010

EPL, **92** (2010) 24003
doi: 10.1209/0295-5075/92/24003

www.epljournal.org

Dynamical facilitation decreases when approaching the granular glass transition

R. Candelier[1], O. Dauchot[1(a)] and G. Biroli[2,3]

[1] *SPEC, CEA-Saclay, URA 2464 CNRS - F-91191 Gif-sur-Yvette, France, EU*
[2] *Institut de Physique Théorique, CEA, IPhT - F-91191 Gif-sur-Yvette, France, EU*
[3] *CNRS, URA 2306 - F-91191 Gif-sur-Yvette, France, EU*

received 1 July 2010; accepted in final form 6 October 2010
published online 17 November 2010

PACS 45.70.Mg – Granular flow: mixing, segregation and stratification
PACS 45.70.Ht – Avalanches
PACS 61.43.-j – Disordered solids

Abstract – We investigate the relaxation dynamics of a dense monolayer of bidisperse beads by analyzing the experimental data previously obtained in a fluidized bed. We demonstrate that dynamical facilitation becomes less conserved and plays a lesser role for the structural relaxation when approaching the glass transition. We first show that the dynamics obeys the same elementary processes as those previously reported in a cyclic shear experiment: cage jumps aggregate on a very short time into clusters. We then show that increasing the packing fraction makes the spatio-temporal organization of these clusters evolve from a rather scattered and random distribution towards a collection of sparse and finite avalanche events.

Copyright © EPLA, 2010

Introduction. – The dynamics of supercooled liquids [1,2], colloids [3] and agitated granular media [4] dramatically slows down as these systems are cooled down or compressed, while the particles configurations remain similar to those of a fast relaxing liquid. Instead the dynamics do show significant modifications: there is by now experimental [3,5–10] and numerical evidence [11–16] that the dynamics becomes spatially heterogeneous. Providing a microscopic explanation for this phenomenology, refered to as the glass transition in the case of thermal systems, has become a central issue [17–21]. Despite a number of theoretical proposals [22–27], there is still no consensus about the microscopic mechanisms responsible for it.

One particularly debated question is the role of dynamical facilitation (DF) in glassy dynamics. DF means that a local relaxation has a very high probability of happening nearby another relaxation after a certain time, which is short compared to the macroscopic relaxation time but large compared to the microscopic one. Effective models based on kinetic constraints [26,28] posit that DF is the underlying cause of particle mobility by assuming that a region of frozen atoms can recover mobility only when it is adjacent to a region already mobile. Within the models this is due to the existence of mobility inducing defects, which cannot disappear (or appear) except if there is another defect nearby. This constraint implies that local relaxations cannot start or end without correspondingly being preceded or followed in space and time by other local relaxations. We will refer to this property as *conservation* of DF. In other approaches [29], instead, DF is an important piece of the theoretical description but not the driving mechanism of glassy dynamics.

Athermal systems such as colloids and granular media are in principle very different from supercooled liquids. Still, there are mounting evidences that their glassy dynamics are very similar and the study of such athermal systems have proven in the past to be very useful in illustrating the microscopic mechanisms responsible for dynamical arrest [3,7,9,10,30]. Visual observations in colloids [31], granular media [32–34] and numerical simulations of supercooled liquids [30,35] reveal that the motion becomes intermittent at the microscopic scale: typically a particle rattles for a long time inside a "cage" formed by its neighbours, before jumping into another "cage". Consecutive cage jumps lead to structural relaxation and long time diffusion. Clearly, understanding how consecutive cage jumps conspire together and lead to macroscopic relaxation would be very instrumental in clarifying the role of dynamical facilitation and in explaining the emergence of dynamical heterogeneity.

(a) E-mail: olivier.dauchot@cea.fr

A first attempt in this direction has been made in the study of granular media [34], where we unveiled that dynamical heterogeneities arise from the aggregation of quasi-instantaneous clusters of cage jumps into long-lasting structures. The avalanching process leading to these structures provides a clear evidence of the important role played by DF: a local relaxation due to a cluster of cage jumps is typically followed nearby in space and in time by another cluster relaxation, and so on and so forth. Note that we do not find any other manifestation of DF beyond avalanches[1]: as a consequence it becomes crucial to characterize the evolution of this avalanching process as the dynamics slow down in order to understand more precisely the role played by DF. This is the main goal of the present letter.

Apart from strengthening our previous observations, by reproducing them in a very different system, we demonstrate that dynamical facilitation, present at the onset of the slowing down of the dynamics, becomes less conserved and plays a lesser role approaching the glass transition. This experimental observation could be decisive in discriminating amongst the various theoretical scenarii.

Cage dynamics and relaxation events. – We focus on the $2D$ fluidized bed of beads studied in [9], whose experimental data were generously provided by the authors. The system is made of a $1:1$ bidisperse mixture of N steel beads of diameters $d_S = 0.318\,\mathrm{cm}$ and $d_L = 0.397\,\mathrm{cm}$ $(d_L/d_S = 1.25)$, with respective masses of $0.130\,\mathrm{g}$ and $0.266\,\mathrm{g}$, confined to a circular cell of diameter $17.7\,\mathrm{cm} = 55.7 d_S$. Bead motion is excited by an upward flow of air at a fixed superficial flow speed of $545 \pm 10\,\mathrm{cm\,s^{-1}}$ (resp. $500 \pm 10\,\mathrm{cm\,s^{-1}}$) for the 3 loosest (resp. densest) packing fractions. The original acquisition frame rate is $120\,\mathrm{Hz}$; we retain one frame out of ten and follow the trajectories over 10,800 frames. To avoid boundary effects, we consider a circular region of interest of diameter $D = 45 d_S$. All lengths are expressed in number of small grain diameters, and times in number of frames ($\frac{1}{12}$ s). We study packing fraction ranging from $\phi = 0.758$ to $\phi = 0.802$ ($N = 1790$ to 1975). The data for the three densest packings were not discussed in [9].

The root mean square displacement along the x-axis on a lag time τ, $\sigma_x(\tau)$ (fig. 1, top right) shows all the well-known characteristics observed when approaching the glass transition: a sub-diffusive plateau at intermediate time scales, which enlarges when increasing the packing fraction, and the final recovery of a diffusive regime on long times[2]. A common interpretation is to attribute sub-diffusion to cage trapping (see fig. 1, top left) and long-term diffusion to successive jumps between cages (see *e.g.* [9,31,36]). In order to characterize more quantitatively the microscopic relaxation processes, we apply the same procedure as developed in [34] which allows one to extract the spatio-temporal location of cage jumps (see the "Methods" section at the end of this letter).

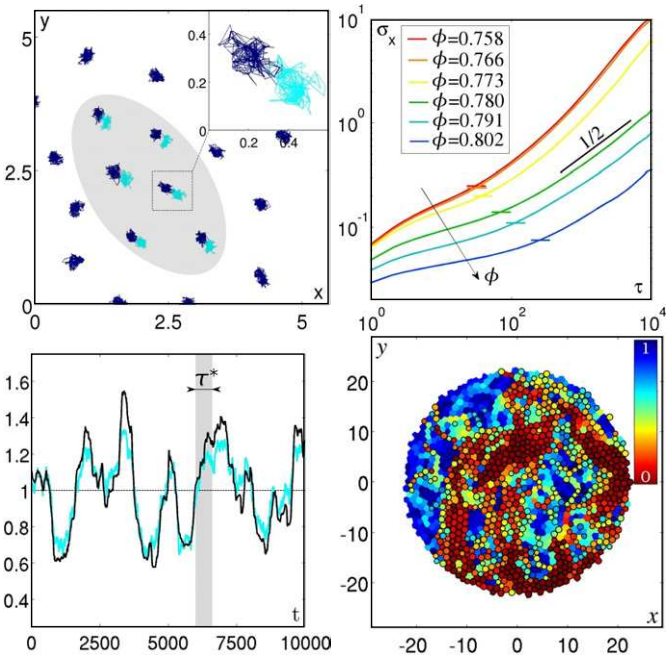

Fig. 1: (Color online) Dynamics and cooperative jumps. Top-left: trajectories of a few particles at $\phi = 0.802$ for 1000 time frames. The color changes from blue (black) to cyan (light grey) when a cage jump is detected. All cage jumps in the grey area appear within 15 time steps, defining a cooperative cluster. Top-right: root mean square displacement along the x-direction $\sigma_x(\tau)$ for the 6 packing fractions $\phi = 0.758$ (red) to 0.802 (blue). The horizontal dashes indicate σ_c the crossover from the sub-diffusive to the diffusive regime. Bottom-left: comparison between the relative averaged relaxation $Q_t/\langle Q_t\rangle_t$ in cyan (light grey) and the relative percentage $P_t(\tau^*)/\langle P_t\rangle_t$ of particles that have not jumped between t and $t+\tau^*$ in black, at $\phi = 0.773$ ($\tau^* = 611$). The grey area represent the lag for which the dynamics is plotted on the right. Bottom-right: representative example of the spatial field of the two-point correlation function $Q_{p,t}(a^*, \tau^*)$. Particles jumping between t and $t+\tau^*$ are surrounded by a black circle. They largely cover the regions of fast relaxation.

We also check that the non-trivial dynamics is fully encoded in the cage jumps by quantifying the relaxation of the system using the dynamical correlator:

$$Q_{p,t}(a,\tau) = \exp\left(-\frac{||\Delta\vec{r}_p(t,t+\tau)||^2}{2a^2}\right), \qquad (1)$$

where $||\Delta\vec{r}_p(t,t+\tau)||$ is the absolute value of the displacement of particle p between times t and $t+\tau$. Averaging this quantity over all particles, one obtains

[1] One could relate the aggregation of cage jumps in clusters to dynamical facilitation taking place on very short time scales. We note, however, that this would correspond to a kind of DF quite different from the one usually discussed in the current physical literature.

[2] For the three loosest packings the slope is greater than $1/2$, indicating the presence of slow convection rolls. This effect, which becomes stronger at even lower densities, lead us to retain only the highest packing fraction, for which it does not interfere with the time scales of the analysis.

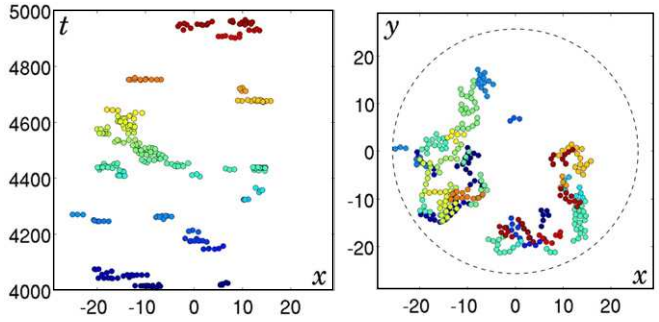

Fig. 2: (Color online) Spatio-temporal vizualisation of the cage jumps in a time window of 1000 time steps at $\phi = 0.791$. On both plots each dot stands for a cage jump and color represents the jumping time. Both plots are made with the same data. Left: one spatial direction and time; right: the two spatial directions. The dotted circle is the boundary of the region of interest. Note that cage jumps aggregate in clusters that are well separated in space and in time.

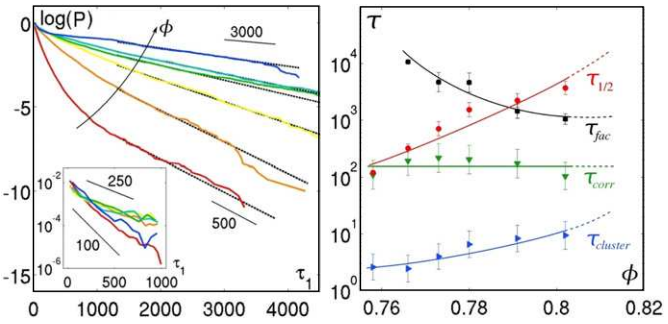

Fig. 3: (Color online) Time scales and their evolution with the packing fraction. Left: distributions of τ, the lag time between adjacent clusters; main plot: $P(\tau > \tau_1)$ —black dotted lines are exponential fits at large τ_1. Inset: Pdf(τ) for the population of short lag times (see text for more details); black lines are indicative exponential decays. Right: τ_{cl} (▶), τ_{corr} (▼), τ_{fac} (■) and $\tau_{1/2}$ (●), which is roughly τ_{cage}. Note that $\tau_{corr} > \tau_{cl}$, confirming that clusters are short, well-defined dynamical events.

$Q_t = \langle Q_{p,t}(a^*, \tau^*)\rangle_p$, where the time and length scales a^* and τ^* are defined such that the dynamical heterogeneities are maximal (see *e.g.* [33] for details on this procedure). We compare the relative $Q_t/\langle Q_t\rangle_t$ with $P_t(\tau^*)/\langle P_t\rangle_t$ the relative percentage of particles that have not jumped during the same lag τ^*: fig. 1, bottom left, shows that the correspondence is excellent, revealing that the bursts of cage jumps localized by the algorithm are responsible for the major relaxation events of the system. One can also check that the cage jumps are exactly located in the areas where the decorrelation is maximal (see *e.g.* fig. 1, bottom right).

Spatio-temporal distribution of cage jumps. – We find that cage jumps are not randomly distributed in space and time but rather aggregate into cooperative clusters (see fig. 2 for a spatio-temporal illustration and the "Methods" section for an explicit definition of the clusters). The very short duration of clusters, denoted τ_{cl}, is small compared to all the other time scales of the dynamics. These clusters can thus be considered as instantaneous events. The number of particles involved in these cooperative clusters is roughly power law distributed, with a cut-off at the system's size (see fig. 5, left). This observation suggests that these elementary events of the dynamics do not have a well-defined average size.

Subsequent clusters of cage jumps are not uniformly distributed in space and time either, as suggested for instance in fig. 2, right. Instead, our analysis reveals that a cluster typically is followed nearby in space and in time by another cluster. The aggregation of these events leads, on a longer time scale, to structural relaxation. Clusters are defined as adjacent in space if they are separated by less than $r_{th} = 1.5$ when projected on a single time frame. Moreover, we record the lag times τ separating adjacent clusters (see the "Methods" section for more details). Figure 3, top, displays $P(\tau > \tau_1)$, the probability of observing τ larger than τ_1; these cumulated distributions are well described by the addition of two processes:

$$P(\tau > \tau_1) = \left(p_{corr} e^{-\frac{\tau_1}{\tau_{corr}}} + (1 - p_{corr}) e^{-\frac{\tau_1}{\tau_{cage}}}\right), \quad (2)$$

where p_{corr} is the fraction of short lag times. The short time scale τ_{corr} physically reveals the existence of correlated clusters and we observe that the long time scale τ_{cage} corresponds to the average time spent in a cage. We first extract τ_{cage} and p_{corr} by fitting the large τ_1 regime, then subtract the large τ_1 contribution and obtain the exponential distribution for the short lag times —displayed in the inset of fig. 3, top left— and from which one easily estimates τ_{corr}. When $\tau_{cage} \gg \tau_{corr}$, one can also identify sets of correlated clusters adjacent in space and in time. These sets, that we call *avalanches*, last for a time τ_{fac} during which dynamical events correlate to previous dynamical events nearby, which is a particular way to construct dynamic heterogeneity, namely dynamical facilitation. These important observations are qualitatively identical to those reported in [34] and confirm the robustness of both the analysis and the physical phenomena.

Towards the dynamical transition. – We now come to the central discussion of this work: the evolution of the above dynamical patterns, when the packing fraction is increased towards the glass transition. One observes on fig. 3, right, that the short duration τ_{cl} of the cooperative clusters varies from 2 to 10 with the packing fraction, not a significant variation given our temporal resolution on the detection of the cage jumps. Also, τ_{corr} does not vary much, it remains bounded between 100 and 250 without clear tendency. Instead, τ_{fac} decreases with ϕ while τ_{cage} matches the structural relaxation time or its alternative estimation $\tau_{1/2}$, the time needed for observing half the particles jump once, which increases from 511 to 3041.

Let us now discuss the physical consequences of these findings. Clearly, the picture of clusters dynamically

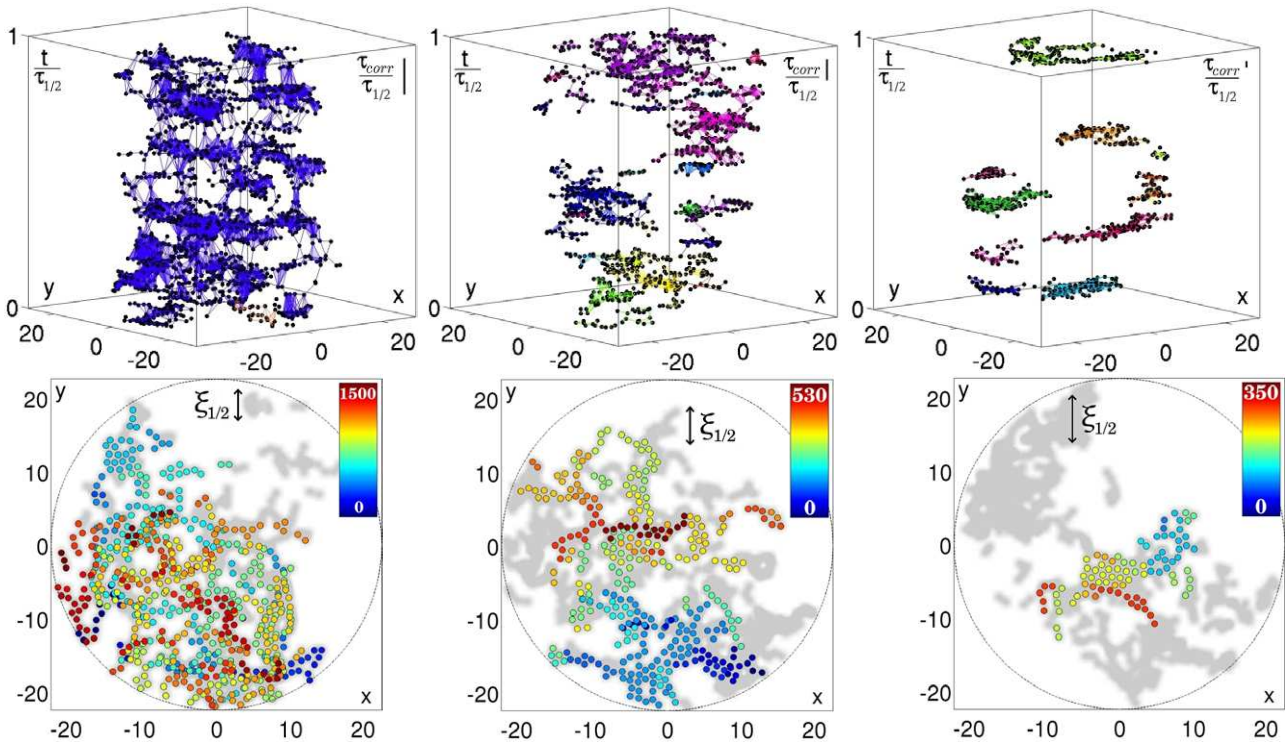

Fig. 4: (Color online) Top: mobility patterns in space and time during the typical relaxation time $\tau_{1/2}(\phi)$ for 3 packing fractions: from left to right $\phi = 0.780$, 0.791, 0.802 and $\tau_{1/2} = 1540$, 2250, 3730. The two directions of space are in the horizontal plane and time is the vertical axis. The ratio $\tau_{corr}/\tau_{1/2}$ is given in the upper-right corners. Jumps are represented with black dots, and all possible tetrahedrons, whose edges are the links between correlated jumps, are shown, forming volumes. Each separate connected structure has a different color. Bottom: jumps occurring in $\tau_{1/2}$ (in grey), same packing fractions. The jumps belonging to one arbitrarily chosen connected structure are colored according to the time at which they occur.

facilitating each others only makes sense when τ_{cage} is larger than τ_{corr}, that is above $\phi^* \sim 0.77$, which would be analogous to the onset temperature in supercooled liquids. The way in which clusters aggregate and the resulting mobility patterns are represented in fig. 4, top, for three packing fractions in 3D space/time, the time axis being rescaled with respect to the relaxation time $\tau_{1/2}$. We draw all cage jumps (black dots) and link all pairs of jumps that are separated by less than τ_{corr} in time and $r_{th} = 1.5$ in space. This defines a network whose vertices are the cage jumps and whose edges are the orientated links between correlated jumps.

For the loosest packing fraction, connected jumps form a highly interconnected monolith: $\tau_{fac} \gg \tau_{1/2}$ and dynamical facilitation is conserved on time scales relevant for structural relaxation. When raising ϕ, an increasing number of adjacent clusters become separated by more than a few τ_{corr} within a time interval equal to the relaxation time ($\tau_{1/2}/\tau_{corr} \simeq \tau_{cage}/\tau_{corr}$ increase up to 30). Concomitantly, τ_{fac} decreases, and becomes smaller than $\tau_{1/2}$ for the largest ϕ. For this density, several independent avalanches start and end within a time interval of the order of the relaxation time scale and facilitation is clearly not conserved anymore. We also find that p_{corr} decreases from 90% to 40%, indicating that avalanches are composed of a decreasing relative number of clusters. The above observations suggest that at even higher density τ_{fac} might become of the order of τ_{corr}: each avalanche would reduce to a single cluster.

The above evolution of the time scales strongly influences that of the associated length scales. The bottom panel of fig. 4 displays the spatial projection of all cage jumps during $\tau_{1/2}$. In grey, one sees all the particles which have jumped, which correspond by definition to half of the total number of particles. The jumps belonging to one arbitrarily chosen avalanche are colored according to the time at which they occur. The typical size of clusters ξ_{cl} and the dynamical correlation length scale $\xi_{1/2}$ are given by the average width of the backbone forming the mobility pattern over τ_{cl} and $\tau_{1/2}$, respectively, see the "Methods" section for a description of how these length scales are extracted. For the lowest ϕ (left panel) $\tau_{fac} > \tau_{1/2}$ and almost all cage jumps belong to the same large, eventually infinite connected structure. $\xi_{1/2}$ is roughly the cluster size, thus showing that the pattern is formed by dynamically independent clusters. At higher ϕs, the distributions of the cluster sizes n_c (see fig. 5, left) have larger tails and their experimental average $\langle n_c \rangle$ grows from 3.4 to 5. However the typical width of clusters backbones ξ_{cl} almost does not vary with the packing fraction in the studied regime, as shown in fig. 5, right. Instead, the dynamical correlation length scale $\xi_{1/2}$, increases sharply for larger

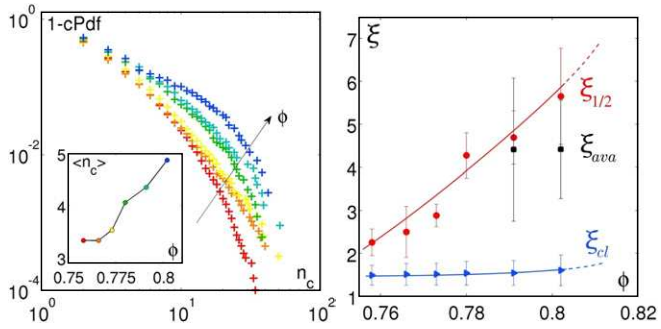

Fig. 5: (Color online) Length scales as functions of the packing fraction. Left: cumulated Pdf of the clusters' number of particles n_c for the 6 packing fractions $\phi = 0.758$ (red) to 0.802 (blue); Inset: mean value of n_c over all clusters, as a function of ϕ. Right: ξ_{cl} (▶), $\xi_{1/2}$ (●) and ξ_{ava} (■). Plain lines are guides for the eyes, dashed lines are extrapolations.

ϕ. The natural interpretation is that until ϕ^* the mobility pattern is so much intertwined that a cluster is facilitated by several others and dynamical correlations do not propagate farther than the size of one single cluster. For the packing fraction corresponding to the middle panel of fig. 4, bottom, $\tau_{fac} \simeq \tau_{1/2}$ and the dynamical heterogeneities match the avalanches, hence $\xi_{1/2} = \xi_{ava}$. For the largest packing fraction the avalanche size seems to decrease while $\xi_{1/2}$ is still increasing. Note that it is really the nature of the clusters aggregation which changes with density. From a very much interwined structure at low density, it evolves for large densities towards avalanches well separated from each other and from the boundaries of the observation volume. As a consequence, there is no rescaling in space of these patterns.

Conclusion. – To summarize, analyzing data coming from a fluidized monolayer experiment, we have confirmed the predominant role of the spatio-temporal organization of cage jumps in the relaxation dynamics previously pointed out in our cyclic shear experiment, and revealed its evolution with the packing fraction. Above a characteristic packing fraction, akin to the onset temperature in liquids, facilitation starts to play a role in the dynamics. Then, increasing the packing fraction, mobility patterns evolve from a single connected structure spanning the experimental time to isolated denser avalanches of finite size and duration. Dynamical correlations are, at first, of the size of clusters and then, in the latter regime, of the size of the avalanches. The cluster size increases with the packing fraction whereas the number of correlated clusters inside an avalanche decreases. Thus the cooperative relaxation of the first cluster of an avalanche plays a larger role and facilitation a lesser one. Identifying the mechanisms responsible for the dynamical heterogeneities at the largest packing fractions and how avalanches appear/disappear, as well as investigating whether the above findings also hold for supercooled liquids would certainly be of great interest.

Methods. – First, we describe how the cage jumps locations in space and time are extracted from the individual dynamics. For that purpose, we introduce a measure of the square distance separating two subsets of a given trajectory:

$$\forall t \in [t_i, t_f], \quad \tilde{p}(t) = \sqrt{\langle d_1(t_2)^2 \rangle_{t_2 \in S_2} . \langle d_2(t_1)^2 \rangle_{t_1 \in S_1}},$$

where t_i and t_f are the initial and final times of the trajectory, $S_1 = \{t_i; t\}$ and $S_2 = \{t; t_f\}$ are the two subsets of points before and after time t, $d_i(t_j)$ stands for the Euclidian distance from the position at t_j to the center of mass of the subset S_i, and $\langle . \rangle_{t_j \in S_j}$ denotes an average over the subset S_j. $\tilde{p}(t)$ is therefore the product of the root mean square distances between all the points of the subsets to the barycenter of the *other* subset. In order to have a well defined $\tilde{p}(t)$, there must be enough points in each subset to approximate the barycenter's position accurately, which is not true close to the bounds t_i and t_f; it is thus convenient to introduce $p(t) = \xi(t).\tilde{p}(t)$ where $\xi(t) = \frac{2[(t_f - t)(t - t_i)]^{1/2}}{t_f - t_i}$ is a natural normalization of $\tilde{p}(t)$, which counterweights the lack of statistics in the subsets defined close to the extremities of the trajectory. Then, the cage jumps are identified by considering the dependence of $p(t)$ *vs.* t, which peaks at the time at which the centers of mass are best separated, thereby identifying the cage jumps. In the case where the motion entirely takes place in a single cage, the barycenters of any two subsets remain close to each other, leading to a roughly constant $\tilde{p}(t) \simeq \sigma_c^2$, where σ_c is the typical size of the cage. Then, the algorithm consists of an iterative procedure; initially the whole trajectory is taken, and two "branches" are created each time a jump is located, corresponding to the sub-trajectories before and after the jump. A branch stops as soon as no value of $p(t)$ stands above the natural threshold $p_{th} = \sigma_c^2$, where σ_c is the length scale of the crossover at which the root mean square displacement recovers a diffusive regime (see fig. 1, top right). By construction p_{th} is the lower bound for the jump amplitudes.

The major advantage of the above algorithm is that the duration of the jump does not come into play. Only the separation of the cages determines the existence of a jump, as it should be. In essence the robustness of this algorithm comes from the fact that the cages are statistically much better defined than the jumps. Note that the case of two consecutive jumps in opposite direction is not an issue for this algorithm because the average time between consecutive jumps is orders of magnitude above the jumping time itself. We have checked on artificial trajectories mimicking the cage effect that the algorithm is very close to detect all cage jumps perfectly: the number of false-positive is roughly constant and around 1%. In addition, the temporal location of the jumps is excellent: the standard deviation of the lags between the real jumps and their matches is always smaller than 4 time steps.

Second, we explain how clusters and avalanches are defined and determined. Two cage jumps belong to the

same cluster if they are separated in time by less than a temporal threshold t_{th} and distant from less than a distance threshold r_{th}. The temporal threshold t_{th} is set to be the 4 time steps resolution of the cage jumps separation algorithm. Varying the distance threshold r_{th}, one observes a plateau in the dependance of the number of clusters detected by the algorithm as a function of r_{th}. We select $r_{th} = 1.5$ in the center of this plateau in such a way that the output of the clusterizing procedure is fairly robust. Avalanches ("clusters of clusters") are determined with the same two-thresholds procedure, the time threshold being the correlation time τ_{corr} while the distance threshold remains the same as above.

We finally discuss how the different time and length scales are computed. τ_{cl} is the average value of the clusters' durations, *i.e.* the lags separating the first and last jumps of a cluster. These lags are exponentially distributed. τ_{cage} and τ_{corr} are extracted by fitting the cumulated distributions $P(\tau > \tau_1)$ with eq. (2). $\tau_{1/2}$ is the average time needed so that half the particles in the region of interest have jumped. τ_{fac} corresponds to the average duration of the avalanches, *i.e.* the lags between the first and the last cage jumps among all the clusters of an avalanche. The length scales ξ_{cl} and ξ_{ava} are extracted from the projections of the corresponding spatio-temporal objects onto the 2D spatial plane. The latter is divided in pixels of lateral size $d_S/10$, set to 1 if part of an object projects on it and 0 otherwise. The lenght scales are computed as the typical "width" of the pattern made of the pixels set to 1. The "width" of such a pattern is defined as the average length of the distinct segments made of successive pixels inside the pattern. $\xi_{1/2}$ is computed the same way, the corresponding spatio-temporal pattern being the ensemble of jumps occuring until half the system has jumped at least once. ξ_{cl}, ξ_{ava} and $\xi_{1/2}$ are averaged on all possible realizations of the corresponding patterns.

* * *

We thank A. R. Abate and D. J. Durian for sharing their data and J.-P. Bouchaud, D. R. Reichman and L. Berthier for feedback on this paper. This work was supported by ANR DYNHET 07-BLAN-0157-01.

REFERENCES

[1] Ediger M. D., Angell C. A. and Nagel S. R., *J. Phys. Chem.*, **100** (1996) 13200.
[2] Debenedetti P. G. and Stillinger F. H., *Nature*, **410** (2001) 259.
[3] Weeks E. R., Crocker J. C., Levitt A. C., Schofield A. and Weitz D. A., *Science*, **287** (2000) 627.
[4] Dauchot O., in *Ageing and the Glass Transition*, edited by MPRS, Vol. **4** (Springer) 2007, p. 161.
[5] Ediger M. D., *Annu. Rev. Phys. Chem.*, **51** (2000) 99.
[6] Berthier L., Biroli G., Bouchaud J.-P., Cipelletti L., El Masri D., L'Hote D., Ladieu F. and Pierno M., *Science*, **310** (2005) 1797.
[7] Dauchot O., Marty G. and Biroli G., *Phys. Rev. Lett.*, **95** (2005) 265701.
[8] Lechenault F., Dauchot O., Biroli G. and Bouchaud J.-P., *EPL*, **83** (2008) 46003.
[9] Keys A. S., Abate A. R., Glotzer S. C. and Durian D. J., *Nat. Phys.*, **3** (2007) 260.
[10] Cipelletti L. and Ramos L., *J. Phys.: Condens. Matter*, **17** (2005) R253.
[11] Hurley M. M. and Harrowell P., *Phys. Rev. E*, **52** (1995) 1694.
[12] Kob W., Donati C., Plimpton S. J., Poole P. H. and Glotzer S. C., *Phys. Rev. Lett.*, **79** (1997) 2827.
[13] Bennemann C., Donati C., Baschnagel J. and Glotzer S. C., *Nature*, **399** (1999) 246.
[14] Lacevic N., Starr F. W., Schroder T. B. and Glotzer S. C., *J. Chem. Phys.*, **119** (2003) 7372.
[15] Doliwa B. and Heuer A., *Phys. Rev. E*, **61** (2000) 6898.
[16] Whitelam S., Berthier L. and Garrahan J. P., *Phys. Rev. Lett.*, **92** (2004) 185705.
[17] O'Hern C. S., Silbert L. E., Liu A. J. and Nagel S. R., *Phys. Rev. E*, **68** (2003) 11306.
[18] Andersen H. C., *Proc. Natl. Acad. Sci. U.S.A.*, **102** (2005) 6686.
[19] Zhang Z., Xu N., Chen D. T. N., Yunker P., Alsayed A. M., Aptowicz K. B., Habdas P., Liu A. J., Nagel S. R. and Yodh A. G., *Nature*, **459** (2009) 230.
[20] Berthier L. and Witten T. A., *Phys. Rev. E*, **80** (2009) 021502.
[21] Liu A. J. and Nagel S. R., *Jamming and Rheology: An Introduction* (Taylor & Francis) 2001, p. 385.
[22] Tarjus G., Kivelson S. A., Nussinov Z. and Viot P., *J. Phys.: Condens. Matter*, **17** (2005) 1143.
[23] Shintani H. and Tanaka H., *Nat. Phys.*, **2** (2006) 200.
[24] Lubchenko V. and Wolynes P. G., *J. Chem. Phys.*, **121** (2004) 2852.
[25] Biroli G., Bouchaud J.-P., Cavagna A., Grigera T. S. and Verrocchio P., *Nat. Phys.*, **4** (2008) 771.
[26] Garrahan J. P. and Chandler D., *Phys. Rev. Lett.*, **89** (2002) 035704.
[27] Brito C. and Wyart M., *J. Stat. Mech.* (2007) L08003.
[28] Fredrickson G. and Andersen H., *Phys. Rev. Lett.*, **53** (1984) 1244.
[29] Bhattacharyya S. M., Bachi B. and Wolynes P. W., *Proc. Natl. Acad. Sci. U.S.A.*, **105** (2008) 16077.
[30] Candelier R., Widmer-Cooper A., Kummerfeld J. K., Dauchot O., Biroli G., Harrowell P. and Reichman D. R., *Phys. Rev. Lett.*, **105** (2010) 135702.
[31] Weeks E. R. and Weitz D. A., *Phys. Rev. Lett.*, **89** (2002) 95704.
[32] Pouliquen O., Belzons M. and Nicolas M., *Phys. Rev. Lett.*, **91** (2003) 014301.
[33] Marty G. and Dauchot O., *Phys. Rev. Lett.*, **94** (2005) 15701.
[34] Candelier R., Dauchot O. and Biroli G., *Phys. Rev. Lett.*, **102** (2009) 088001.
[35] Kudchadkar S. R. and Wiest J. M., *J. Chem. Phys.*, **103** (1995) 8566.
[36] Doliwa B. and Heuer A., *Phys. Rev. Lett.*, **80** (1998) 4915.